

NASA TECHNICAL  
MEMORANDUM



NASA TM X-3247

NASA TM X-3247

EFFECT ON FAN FLOW CHARACTERISTICS  
OF LENGTH AND AXIAL LOCATION  
OF A CASCADE THRUST REVERSER

*Donald A. Dietrich, Andrew J. Crooker,  
and Gary G. Kelm*

*Lewis Research Center  
Cleveland, Ohio 44135*



NATIONAL AERONAUTICS AND SPACE ADMINISTRATION • WASHINGTON, D. C. • JUNE 1975

1. Report No. <b>NASA TM X-3247</b>		2. Government Accession No.		3. Recipient's Catalog No.	
4. Title and Subtitle <b>EFFECT ON FAN FLOW CHARACTERISTICS OF LENGTH AND AXIAL LOCATION OF A CASCADE THRUST REVERSER</b>				5. Report Date <b>June 1975</b>	
				6. Performing Organization Code	
7. Author(s) <b>Donald A. Dietrich, Andrew J. Crooker, and Gary G. Kelm</b>				8. Performing Organization Report No. <b>E-8223</b>	
9. Performing Organization Name and Address <b>Lewis Research Center National Aeronautics and Space Administration Cleveland, Ohio 44135</b>				10. Work Unit No. <b>505-05</b>	
				11. Contract or Grant No.	
12. Sponsoring Agency Name and Address <b>National Aeronautics and Space Administration Washington, D.C. 20546</b>				13. Type of Report and Period Covered <b>Technical Memorandum</b>	
				14. Sponsoring Agency Code	
15. Supplementary Notes					
16. Abstract <p>A series of static tests were conducted on a model fan with a diameter of 14.0 cm to determine the fan operating characteristics, the inlet static pressure contours, the fan-exit total and static pressure contours, and the fan-exit pressure distortion parameters associated with the installation of a partial-circumferential-emission cascade thrust reverser. The tests variables included the cascade axial length, the axial location of the reverser, and the type of fan inlet. It was shown that significant total and static pressure distortions were produced in the fan aft duct, and that some configurations induced a static pressure distortion at the fan face. The amount of flow passed by the fan and the level of the flow distortions were dependent upon all the variables tested.</p>					
17. Key Words (Suggested by Author(s)) <b>Thrust reversers                      Cascades</b> <b>Thrust reversing                      Model testing</b> <b>Propulsion systems</b>				18. Distribution Statement <b>Unclassified - unlimited</b> <b>STAR Category 07 (rev.)</b>	
19. Security Classif. (of this report) <b>Unclassified</b>		20. Security Classif. (of this page) <b>Unclassified</b>		22. Price* <b>\$3.75</b>	
		21. No. of Pages <b>36</b>			

\* For sale by the National Technical Information Service, Springfield, Virginia 22151

# EFFECT ON FAN FLOW CHARACTERISTICS OF LENGTH AND

## AXIAL LOCATION OF A CASCADE THRUST REVERSER

by Donald A. Dietrich, Andrew J. Crooker\*, and Gary G. Kelm

Lewis Research Center

### SUMMARY

A series of static tests were conducted on a model fan to determine the fan operating characteristics, the inlet static pressure contours, the fan-exit total and static pressure contours, and the fan-exit pressure distortion parameters associated with the installation of a partial-circumferential-emission cascade thrust reverser. The work was performed using a model fan which was 14.0 centimeters in diameter and passed a fan mass flow of about 2.5 kilograms per second at an approximate fan pressure ratio of 1.25 at the design fan rotational speed of 35 800 rpm. The test series included nine configurations of a cowl cascade thrust reverser all of which had a total circumferential emission angle of  $241.2^{\circ}$ . The test variables included the axial cascade length, the axial location of the reverser, and the type of fan inlet. It was shown that total and static pressure distortions did exist at the fan exit and that some configurations induced a static pressure distortion at the fan face. The amount of flow passed by the fan and the level of the distortion were dependent upon all the variables tested.

### INTRODUCTION

The application of thrust reversing to short-haul aircraft operation differs from the case of conventional aircraft because of the shorter field length, higher thrust-to-weight ratio, and lower landing speeds of short-haul aircraft. The thrust reverser must be similar to those on present conventional aircraft in that it must generate sufficient reverser thrust to stop the aircraft, minimize the additional required weight, eliminate

---

\*Assistant Professor of Aerospace Engineering, San Diego State College, San Diego, California; Summer Faculty Fellow at the Lewis Research Center in 1971 and 1972.

reingestion of hot exhaust flow, and avoid jet impingement on the ground. During the period of reversing, neither the engine operating point nor internal flow quality should be adversely affected to an extent that would result in reduced stall margin, reduced thrust, increased fan noise, and increased blade vibrational stress.

High thrust-reversing efficiency in conjunction with the relatively high installed thrust-to-weight ratio of short-haul aircraft can be used to advantage in reducing reverser-related noise and in meeting the aircraft performance requirements. Reference 1 showed that high thrust reverser efficiency can be achieved with a model partial-emission cascade thrust reverser, while reference 2 presents the acoustic characteristics of model cascade thrust reversers. This reference showed that reverser noise is a function of exhaust flow pressure ratio, cascade geometry, and reverser efficiency and that reverser noise levels can be very significant.

The application of a high efficiency cascade reverser to an aircraft to achieve a short stopping distance and low noise is presented in reference 3 based on test data from model thrust reversers such as those reported in references 1 and 2. The results of reference 3 indicate that cascade thrust reversers should be capable of meeting the reverse-thrust and noise requirements for short-haul aircraft application. However, that reference considered only briefly the effect of cascade reverser variables on the internal flow of the model fan. This report presents a more comprehensive detailed discussion of fan internal flow while operating with the cascade thrust reverser investigated in reference 3.

Reference 1 showed that a model partial-emission cascade thrust reverser produces large circumferential variations in the static pressure in the aft fan duct during operation of the thrust reverser. Furthermore, both references 4 and 5 show that a cascade reverser having large circumferential blockage can induce a significant fan flow distortion and back pressure. Thus, the effects of reverser operation on the fan flow appears to be a significant additional consideration.

The purpose of the program discussed in this report was the determination of fan overall operating characteristics, inlet static pressure contours, fan exit total and static pressure contours, and fan exit pressure distortion parameters due to the operation of a partial-emission cascade thrust reverser. Using a model fan which was 14.0 centimeters in diameter and had a design pressure ratio of 1.25, tests were performed on nine thrust reverser configurations each of which had the same geometric emission pattern and a total circumferential emission angle of  $241.2^\circ$ . Fan performance and internal flow distortion are reported for variations in the axial length of the cascade at two axial distances from the fan and for two types of fan inlets with and without a recirculation shield between the inlet and reverser. All tests were performed statically over a range of fan rotational speed from 60 to 100 percent of the fan design speed.

## SYMBOLS

$A$	area, $m^2$
$A_a$	fan disk area, $6.13 \times 10^{-2} m^2$
$A_{ex}$	exit area, $m^2$
$A_f$	fan face annular area, $5.32 \times 10^{-2} m^2$
$b_c$	reverser length (distance from cascade inlet to blocker door), m
$b_s$	stator spacing distance (distance from stator exit to cascade inlet), m
$D_{ff, max}$	fan inlet static pressure distortion parameter ((maximum static pressure - minimum static pressure)/average static pressure)
$D_s$	stator exit static pressure distortion parameter (standard deviation of static pressure/average static pressure)
$D_{s, max}$	stator exit static pressure distortion parameter ((maximum static pressure - minimum static pressure)/(average static pressure))
$D_t$	stator exit total pressure distortion parameter (standard deviation of total pressure/average total pressure)
$D_{t, max}$	stator exit total pressure distortion parameter ((maximum total pressure - minimum total pressure)/average total pressure)
$d$	passage diameter in reverser section, 15.2 cm
$L$	length of flight-type inlet, 1.9 cm
$\dot{m}$	fan mass flow, kg/sec
$N$	fan rotational speed, rpm
$N_d$	design fan rotational speed, 35 800 rpm
$P$	total pressure, $N/m^2$
$p_o$	ambient pressure, $N/m^2$
$p_s$	static pressure, $N/m^2$
$X$	axial dimension, m
$Y$	radial dimension, m
$\alpha$	circumferential angle, deg
$\delta$	ambient pressure ratio (ambient pressure in $N/m^2/1.013 \times 10^5 N/m^2$ )
$\theta$	ambient temperature ratio (ambient temperature in K/288.2 K)

## Subscripts:

- 1 fan inlet station
- 2 stator exit station
- 3 cascade exit station

## APPARATUS AND PROCEDURE

### Thrust Reverser Model

Figures 1, 2, and 3 presents photographs and sketches of the model fan and nacelles with the cascade thrust reverser used in this test series. Figure 1(a) is a photograph of the forward-thrust configuration which was used as a reference case for the reverse-thrust data. Figure 1(b) shows a reverse thrust configuration. Details of the fan and inlets were presented in reference 1 and are reviewed briefly here.

Fan. - The fan rotor had a tip diameter of 14.0 centimeters, and at the design rotational speed of 35 800 rpm, passed a mass flow of 2.49 kilograms per second at a pressure ratio of 1.25. The fan was driven by a tip turbine which, at the fan design speed, required a mass flow of 0.47 kilogram per second of unheated air at a turbine-plenum pressure of 2590 kilonewtons per square meter. Further information on the basic fan were reported in references 1, 6, 7, and 8.

Inlets. - Two inlet arrangements were used during the test series: a flight-type inlet shown in figure 2(a) and a bellmouth inlet shown in figure 3. The flight-type inlet, shown in detail in figure 4, had a lip made up of quadrants of two 2-to-1 ellipses and an inlet contraction ratio (highlight-to-throat area ratio) of 1.29. With the flight-type inlet installed, the cowl from inlet highlight to stator exit had a length of 1.02 fan tip diameters (fig. 2(a)). The bellmouth (fig. 3) was located 4.3 fan duct diameters forward of the fan stator exit plane and connected to the fan by a cylindrical passage.

Thrust reverser section. - The thrust reverser section (fig. 2(b)) consisted of eight replaceable cascade sectors and two axial support rails located  $180^{\circ}$  apart. Each cascade sector subtended a circumferential angle of  $42.5^{\circ}$  and was replaceable by a solid sector which provided circumferential blockage of the flow. Since each sector contained side walls, the circumferential angle of the flow from each sector was  $40.2^{\circ}$ . This test series was limited to cases where the total emission was through six cascade sectors. In other words, all configurations had two solid (nonflow) sectors as shown in figure 2(b) and a total emission angle of  $241.2^{\circ}$ . The combined fan and drive flow was turned through the cascade reversers by a blocker door which had a forward sloping surface of  $45^{\circ}$  and seals to prevent flow leakage axially. The blocker door was axially

translatable, thus varying the open flow area of the thrust reverser.

Two cascade axial locations were investigated. The close-spacing configuration as shown in figure 2(a) gives the shortest length possible between stator trailing edge and cascade inlet for this model. The second configuration of the model was accomplished by the addition of a spacer which was 6.35 centimeters long as shown in figure 2(c). The addition of the spacer changed the spacing distance, which was the distance from the stator trailing edge to reverser leading edge, from 0.10 to 0.52 fan-duct diameter (i. e.,  $b_s/d = 0.10$  and  $0.52$ ).

The cascade reverser blades, shown in figure 5, were designed to yield a total turning angle from axial of  $135^\circ$ . The blades had a camber of  $110^\circ$ , a chord length of 1.27 centimeters, and a solidity of 1.3. Further details on the design of the thrust reverser are contained in references 1 and 7. Shown in figure 6 is the variation of the calculated reverser exit area ratioed to the annular area at station 2 (stator exit) as a function of both normalized cascade length  $b_c/d$  and the number of open passages between cascade blades. The geometric exit area was calculated by two techniques: basing the exit area on the area approximately normal to the flow direction at station 3 (fig. 5) as in reference 9 and basing the exit area on the cylindrical area at the blade trailing edges projected normal to the mean flow direction as in reference 2. Both curves are given for ease of reference. The flow areas indicated by the symbols correspond to the area for an integral number of blade passages. The effective flow area when the blocker door is between blades has not been estimated. Also indicated on the abscissa are the cascade lengths selected for testing. It was found that geometric flow area ratios substantially greater than 1.0 were required for proper fan operation.

Instrumentation. - The instrumentation used is illustrated in figures 2 and 7. The static taps which measured the fan inlet conditions were located 3.81 centimeters or 0.27 fan diameter upstream of the fan leading edge (fig. 2). These taps were located  $30^\circ$  apart with the first tap offset  $10^\circ$  from the  $0^\circ$  position.

The stator exit station was the primary measuring station and contained the most extensive instrumentation. At this location, there were hub and tip static pressure taps and total pressure rakes. There were seven hub static pressure measurements and twenty tip static pressure measurements with each static tap located circumferentially midway between stator trailing edges. These taps and the total pressure rakes were 0.28 centimeter downstream from the stator trailing edges. However, when the spacer was added, the tip static pressure taps moved 6.35 centimeters downstream as shown in figure 2(c). With or without the spacer, the seven total pressure rakes, as shown in figure 7, were also placed circumferentially midway between stator trailing edges and located 0.28 centimeter downstream from the stator trailing edges. Each rake had six total pressure tubes located at centers of equal areas. However, only five of these were used in reducing the data. The outermost total pressure tube of each rake was

entirely within the turbine exhaust flow and was not used since this study was limited to considerations of the fan performance.

Measurements of the static pressure on the surface of the cylindrical passage immediately downstream of the bellmouth inlet were used to determine the fan mass flow assuming a total pressure recovery of unity in the bellmouth flow. For the case when the flight-type inlet was used, the mass flow measurements from the stator exit station were first correlated to the bellmouth flow measurements, then the stator exit instrumentation was used to determine the mass flow.

### Test Facility

Drive air system. - The drive air system is shown schematically in figure 8. Air from a 3200-kilonewton-per-square-meter compressor passed through a remotely operated globe valve and into two separate air lines. One air line supplied combustion air to a natural gas burner which in turn furnished hot gas for a heat exchanger. The other air line provided indirectly heated drive air to the model fan. A three-way diverting valve, which allowed the drive air to bypass or to flow through the heat exchanger, was positioned by an automatic temperature-control system which maintained a specified temperature at the location of the control thermocouple. Due to heat transfer limitations, the control system was forced to direct all flow through the heat exchanger under the highest flow rate condition, and a gradual drop in drive air temperature occurred with time for some test conditions. A drive air temperature of about 367 K was desired to avoid icing in the drive turbine exit and on surrounding metal parts.

An alternate drive air system was also available throughout the test series. In this system, the drive gas was nitrogen supplied from 15 300-kilonewton-per-square-meter tanks and was coupled through a pressure regulator to the existing drive air line. The burner was then opened using a low pressure combustion air supply. This alternate system had the capability of delivering a higher turbine plenum pressure to the model fan but was not able to provide heated gas for the turbine due to the temperature drop across the pressure regulator associated with the very high supply pressure.

Static test stand. - The static test stand, shown with the model installed in figure 3, was constructed to support the fan, reverser, inlet, and the recirculation shield between the reverser and inlet. The model was connected to a support post by means of a collar and rod which attached to the fan centerbody. The support post stand was bolted to a concrete floor such that the model centerline was located 1.2 meters from the floor. The distance from the model centerline to the concrete side walls was 2.8 meters. The 1.2- by 2.4-meter recirculation shield was used to prevent recirculation of the reversed flow and was located 3.8 fan duct diameters forward of the stator exit plane.



The shield was used with all configurations that included the bellmouth inlet, but was not used with any configuration that included the flight-type inlet.

### Test Configurations

The three variables of the test configurations were the axial cascade length (axial position of the blocker door), the axial distance between the stator and reverser, and the type of inlet. The total emission angle of all the configurations was  $241.2^{\circ}$ , and the geometric arrangement of the emission pattern was fixed. The emission geometry had a single blockage of  $95^{\circ}$  centered about the  $0^{\circ}$  circumferential position plus a small  $10^{\circ}$  blockage at  $180^{\circ}$  (fig. 2(b)). Varying the blocker door position changed the axial length of the cascade section. The five normalized cascade lengths used for the various tests are indicated near the abscissa of figure 5. As stated previously, the values of the normalized stator spacing distance  $b_s/d$  were 0.10 and 0.52. The two types of inlet arrangements were the flight-type inlet and the bellmouth with recirculation shield.

### Test Procedure

For consistency, the same procedure was followed during all tests. The model fan was initially driven at a moderately low rotational speed of approximately 15 000 rpm for 2 minutes to allow the air supply piping to warm. Once the air supply line was heated, it was possible to maintain a reasonably stable turbine plenum temperature throughout the test. Based on information in reference 8, the turbine plenum temperature was selected such that the temperature in the turbine exhaust was between 273 K and room temperature; then the appropriate setting was made on the temperature-control system. The elevated turbine inlet temperature was used so that there would be no ice formation in the fan or turbine exhaust flows. This allowed stable fan flow characteristics throughout the duration of the test. The model fan was then operated with the regulating valve fully open to attain the maximum achievable fan speed, which was less than the fan design speed. At this condition, there was a slow decrease in drive air temperature with time as previously stated. The fan speed was decreased to the desired test levels with three data scans taken at each point. At the lower fan speeds, the temperature control system maintained the desired temperature. In all, thirty-six data scans were taken for each configuration in order to verify data repeatability and the stability of the fan operation.

## RESULTS AND DISCUSSION

The effects of reverser geometry and inlet type on the fan-reverser flow system characteristics are discussed in the following order: overall fan-plus-inlet performance; internal flow static and total pressure profiles; and internal flow distortion parameter.

### Overall Fan-Plus-Inlet Performance

Figures 9 to 13 present the overall fan-plus-inlet performance data for all nine configurations. Shown in figures 9 to 12 are the variations with normalized rotational speed of stator exit average static pressure ratio, mass averaged total pressure ratio, fan equivalent mass flow, and the calculated equivalent exhaust momentum flux, respectively. The data for each of these figures are similarly divided into three parts by configuration so that the first portion of each figure presents the data for all the close-spacing ( $b_s/d = 0.10$ ) configurations, the second portion presents the data for all the extended-spacing ( $b_s/d = 0.52$ ) configurations, and the final portion presents a comparison of the data for the two types of inlets. Figure 13 presents an example of the variation of total pressure ratio with fan corrected mass flow. All of the figures presenting the overall fan-plus-inlet performance include data for the representative forward thrust configuration shown in figure 1(a).

Stator exit static pressure ratio. - Shown in figure 9 is the arithmetic average of the stator exit static pressure measurements ratioed to the ambient pressure as a function of normalized rotational speed  $N/N_d$  for each configuration. This stator exit static pressure ratio represents the back pressure on the fan stage and determines the fan operating point. The data of figures 9(a) and (c) are the average of the hub and tip static pressures while the data of figure 9(b) is the average of the hub static pressures only. However, as will be seen later in figure 14, there is little difference between the hub and tip static pressures so that all the data of figure 9 are comparable. The solid symbols of figure 9 are the data for the representative forward-thrust configuration, and the open symbols are for the reverser configurations.

There is a general trend for the stator exit static pressure to decrease with increasing rotational speed and, as expected, with increasing cascade length (increasing  $b_c/d$ ) or increasing reverser exit area. For the same value of the cascade length parameter  $b_c/d$  increasing the normalized spacing distance  $b_s/d$  from 0.10 to 0.52 significantly decreases the stator exit static pressure as may be seen by comparing figures 9(a) and (b). Also, the flight-type inlet gives a lower stator exit static pressure than the bellmouth inlet plus recirculation shield (fig. 9(c)).

The reverser cascade length may be selected on the basis of having the same stator exit static pressure ratio (the same operating point) during reversing as that of the forward thrust case. Therefore, the cascade length ( $b_c/d$ ) may be selected as 0.58 when the normalized stator spacing distance  $b_s/d = 0.10$  (fig. 9(a)) (as was done in ref. 3) and selected as 0.54 when  $b_s/d = 0.52$ . This indicates that the required reverser cascade length to maintain the same fan operating point is reduced as the stator spacing distance is increased.

Total pressure ratio. - Shown in figure 10 is the mass averaged total pressure at station 2 ratioed to the ambient pressure as a function of normalized rotational speed  $N/N_d$  for each configuration. The total pressure ratio  $P_2/p_o$  is actually the combined pressure ratio of the rotor plus inlet and not the fan stage pressure ratio, since the effect of the stator wakes is not measured by the instrumentation and the total pressure loss of the inlet is included. The total pressure ratio remains essentially unchanged as the cascade length is changed, as shown by the data in figures 10(a) and (b). A comparison of the data of figures 10(a) and (b) shows a small increase in total pressure ratio when the normalized spacing distance is increased from 0.10 to 0.52. The effect of the flight-type inlet (fig. 10(c)) is to significantly reduce the total pressure ratio compared to the bellmouth inlet with recirculation shield. The reduction in total pressure ratio is attributable to a reduction in the inlet pressure recovery associated with the smaller lip radius of the flight-type inlet and possibly also to a small amount of exhaust jet recirculation.

Fan equivalent mass flow. - Shown in figure 11 is the fan equivalent mass flow per unit fan face annular area as a function of normalized rotational speed  $N/N_d$  for each configuration. Contrary to the effect on the total pressure ratio, there is a significant increase in fan mass flow as either the cascade length or the normalized spacing distance is increased. This result is expected since, for these same changes in the cascade length or spacing distance, the stator exit static pressure ratio (or fan back pressure) is decreased. Similar to the case of the total pressure ratio, the effect of the flight-type inlet (fig. 11(c)) is to reduce the fan mass flow compared to the bellmouth inlet with recirculation shield.

Equivalent exhaust momentum flux. - Shown in figure 12 is the calculated ideal exhaust momentum flux as a function of normalized rotational speed  $N/N_d$  for each configuration. The exhaust momentum flux is calculated using the measured fan mass flow and total pressure ratio expanding ideally to ambient conditions. This value is normalized to the standard atmospheric pressure on one ordinate scale. A second scale shows the normalized value divided by the fan disk area. As could be anticipated from the preceding results, there is an increase in ideal exhaust momentum flux as either the cascade length or the normalized spacing distance is increased. Also, as expected, there is a decrease in exhaust momentum flux for the flight-type inlet com-

pared to the bellmouth inlet with recirculation shield.

**Performance map.** - Shown in figure 13 is the variation of the total pressure ratio  $P_2/p_0$  with fan equivalent mass flow per unit fan face annular area  $\dot{m}\sqrt{\theta}/\delta A_f$  for all of the extended-spacing ( $b_g/d = 0.52$ ) configurations. The solid lines which connect the data represent the operating lines for a fixed geometry, and the dashed lines are constant rotational speed lines determined by interpolating between the data points which were at various speeds. It is evident that a decrease in cascade length (exit area) drives the fan in the direction of stall.

In summary, the overall fan-plus-inlet performance characteristics have shown that the cascade acts as a throttle to the fan and there is a need to relate the forward thrust data to the reverse thrust data to establish the proper operating point. In general, a reverser cascade length can be selected in conjunction with a reverser spacing distance which will yield the same fan back pressure, total pressure ratio, and fan mass flow as the forward-thrust case.

### Internal Pressure Profiles

The overall fan-plus-inlet performance characteristics give no information about the internal pressure profiles that occur in the flow. This section considers the significant aspects of the internal flow details when the fan is operated with a cascade thrust reverser.

Shown in figure 14 are the fan inlet static pressures ratios and the stator exit static and total pressure ratios as a function of circumferential position for several of the test configurations. All pressures are ratioed to the measured ambient pressure. Both the extent of the blocked emission and the direction of fan rotation are noted. Each figure also indicates the normalized equivalent fan speed (approximately 35 000 rpm in all cases) and the value of a pressure distortion parameter for each of the pressure profiles. The values of the distortion parameters  $D_{ff, max}$ ,  $D_{s, max}$ , and  $D_{t, max}$  which are defined in the symbol list, are included as a reference in comparing figures.

Figure 14(a) has the general features of all the data presented in figure 14. The fan face static pressure ratios (figs. 14(a-1), (b-1), (c-1), and (d-1) show that a circumferential static pressure variation of about 3 percent fed upstream through the fan. The maximum pressure is displaced angularly  $80^\circ$  in the direction of fan rotation from the center of the blocked emission. The middle part of the figure shows there is approximately a 16 percent stator exit static pressure rise above the average value in the vicinity of the blocked emission. The static pressure has a large variation circumferentially but a comparatively small variation radially. The circumferential variation of the

stator exit total pressure (figs. 14(a-3), (b-3), (c-3), and (d-3)) is similar to that of the stator exit static pressure. However, in the case of the total pressure, there is a significant variation radially. The data from the total pressure probe closest to the tip shows the most dramatic effect with a locally high value in the center of the blocked emission and drop just as the blade leaves the blocked area.

To help visualize the pressure variations of the bottom part of figure 14(a), figure 15 presents those results in the form of contours of constant stator exit total pressure ratioed to the ambient pressure. The locally high total pressure in the center of the blocked region and the low total pressure at the end of the blocked region near the tip are apparent. Also evident is a small shift of the high total pressure region against the direction of blade rotation.

Effect of cascade length. - Figures 14(a) to 14(d) present data for configurations with the close spacing ( $b_s/d = 0.1$ ) showing the effect of increasing the length of the cascade by increasing the value of the cascade length parameter  $b_c/d$  at the design fan speed. As the cascade length is increased, the circumferential and radial variations of the pressure ratios decrease. This result indicates, as noted on the figure, that the distortion parameters decrease with increasing cascade exit area for the close-spacing configurations as the fan operating point is moved away from stall. Figure 14(a) presents the results from the configuration with the shortest cascade length or blocker door position tested. In this case, there were nearly a 3 percent maximum-to-minimum variation of the fan face static pressure, more than a 24 percent variation of the tip total pressure circumferentially, and nearly a 15 percent radial variation of the stator exit total pressure at the location of the blade leaving the blocked region. These values decrease continuously with increasing cascade length (figs. 14(a) to 14(d)) until for a normalized cascade length of  $b_c/d = 0.62$  the distortion values are reduced to 1, 16, and 8 percent, respectively.

Shown in figure 16 is a further analysis of the data used in figure 14(a). In this case, a local static pressure determined from a linear interpolation of the hub and tip static pressures across the flow passage is used to form the local total-to-static pressure ratio. This is shown as a function of circumferential angle. A comparison with the data of figure 14(a) shows the total-to-static pressure ratio is more uniform circumferentially than either the total pressure or the static pressure individually. In addition, these data imply that the local velocity and mass flow are also more uniform circumferentially than the total or static pressures individually.

Effect of cascade location. - Figure 17 presents a set of results similar to those of figure 14 but for the configurations with the spacer installed ( $b_s/d = 0.52$ ). With the spacer installed, there is essentially no variation in the fan inlet static pressure ratios (upper portion of figures) either with circumferential position or with a change in the exit area. The tip static taps at the stator exit are axially displaced by the length of the

spacer (fig. 2(c)). The pressure levels of the displaced static taps (central portion in figure) have the same profile shape as the no-spacer configurations (fig. 14), but the magnitude of the variation is reduced. The static taps at the stator exit location (stator hub, fig. 2(c)) show very little variation. In addition, the stator exit total pressure variations are essentially removed by the additional stator-to-reverser separation. Thus the effect of increased distance to the cascade inlet is to reduce all the internal flow distortion parameters.

Effect of inlet type. - Figure 18 presents the pressure profile data for the configuration which used the flight-type inlet and no recirculation shield. These results when compared with those of figures 14(c) show that the basic characteristics of the pressure profiles are the same as those when the bellmouth and recirculation shield were used. However, the marked increase in the radial and circumferential variations of the stator exit total pressure ratios for positive circumferential angles indicate that some recirculation did occur during the test.

### Stator Exit Distortion Parameters

The internal pressure profiles of the previous section give an indication of the internal flow quality but for only a single rotational speed. This section considers the variation of three stator exit distortion parameters ( $D_s$ ,  $D_t$ , and  $D_{t, \max}$ ) as a function of the normalized rotational speed  $N/N_d$ . The standard deviation of the stator exit static pressures and stator exit total pressures ratioed to the average pressure are  $D_s$  and  $D_t$ , respectively. The parameter  $D_{t, \max}$  is the difference between the maximum and minimum stator exit total pressures ratioed by the mass averaged total pressure.

Effect of cascade length. - The effect of cascade length (cascade exit area) on those configurations which have the close-spacing and the bellmouth inlet plus recirculation shield is shown in figure 19(a). This figure illustrates that the distortion increases linearly with increasing fan speed and that increased cascade length (exit area) reduces all three distortion parameters for the close-spacing configurations.

Effect of cascade location. - Shown in figure 19(b) are data for the configurations with the reverser in the aft location with the bellmouth inlet plus recirculation shield. Comparing these results with those of figure 19(a), it is evident that, when the spacer is added, the cascade length (exit area) has no significant effect on the distortion parameters, and in all cases the distortion level is much reduced. A further characteristic of all the aft-location configurations is that  $D_{t, \max}$  increases sharply with increasing rotational speed at the higher values of rotational speed. The total pressure rake at  $104^\circ$  (fig. 16) showed a radial pressure variation for high fan speeds when the spacer

was installed.

Effect of inlet type. - Figure 19(c) presents the data for the two inlet arrangements. Replacing the bellmouth inlet and recirculation shield with only a flight-type inlet has no effect on the stator exit static pressure distortion. However, the use of the flight-type inlet showed a slight increase in both total pressure distortion parameters over the range of fan speeds tested.

### Design Considerations

Figure 20 presents the fan flow parameters used in this report as a function of the normalized cascade length  $b_c/d$  for all the configurations tested and a constant normalized rotational speed of  $N/N_d = 0.98$ . Shown in figure 20 are the variations of the stator exit average static pressure ratio, fan equivalent mass flow per unit fan face annular area, total pressure ratio, and equivalent ideal exhaust momentum flux along with the corresponding representative data for the forward thrust configuration (fig. 1(a)). As shown previously, the cascade exit area affects primarily the fan stage back pressure and mass flow with little effect on the total pressure ratio. Therefore, the stator exit static pressure ratio may be used in determining the matching conditions of the forward- and reverse-thrust operating points as in reference 3.

As seen in figure 20, increasing the normalized stator spacing  $b_s/d$  results in a decrease in the stator exit static pressure and an increase in both the fan mass flow and exhaust momentum flux. Therefore, in order to match the forward- and reverser-thrust operating points, the close-spacing ( $b_s/d = 0.10$ ) configuration requires a significantly longer cascade length than the extended-spacing ( $b_s/d = 0.52$ ) configuration. However, the total aft cowl length must also be considered in the comparison of the various configurations. The close-spacing configuration does require a longer cascade length ( $b_c/d = 0.58$ ), but has a total aft cowl length ratio  $(b_s + b_c)/d$  of 0.68. The extended-spacing configuration can have a shorter cascade length ( $b_c/d = 0.54$ ), but the total aft cowl length ratio becomes 1.06. Consideration of the total aft cowl length is important since added length due to the reverser would lead to an increase in weight.

Figure 21 presents the stator exit distortion parameters as a function of the normalized cascade length  $b_c/d$  for all the configurations at a constant normalized rotational speed of  $N/N_d = 0.98$ . As shown in figure 21, the close-spacing configurations produce high values of all internal flow distortion parameters. An increase in the internal flow distortion may increase the reverser-related noise which has already been shown in reference 2 to be significant (noise increases with increasing cascade length (cascade exit area)). The extended-spacing configurations tend to reduce the distortion parameters and may reduce the noise due to both reduced cascade length and reduced

fan flow distortion. A compromise between distortion, noise, and weight is required, but is beyond the scope of this report.

## SUMMARY OF RESULTS

A series of static tests were conducted on a model fan with a diameter of 14.0 centimeters to determine the effect on fan flow characteristics of length and axial location of a partial-emission cascade thrust reverser. The main results of this investigation may be summarized as follows:

1. The fan stator exit static pressure ratio, mass averaged total pressure ratio, fan mass flow, and ideal exhaust momentum flux are all functions of the cascade length (exit area), axial distance between stator and reverser, and the type of inlet. A value of the reverser cascade length can be found which gives the same fan operating point for reverse- and forward-thrust operation.
2. The stator exit static pressure has a large circumferential variation for the close-spacing ( $b_s/d = 0.10$ ) configurations. The most extreme case shows a variation in stator-exit static pressure ratio due to the blocked flow area from 0.92 to 1.16. Compared to the circumferential variation, there is little variation radially in the stator exit static pressures for all configurations.
3. For the close-spacing configurations, a circumferential variation in static pressure exists at the fan inlet due to the thrust reverser. The maximum variation is 3 percent.
4. The close-spacing configurations have large radial and circumferential variations in the stator exit total pressure ratio due to the blocked flow area. The maximum local variation is from a total pressure ratio of 1.04 to 1.40 at the fan design rotational speed.
5. The local total-to-static pressure ratio is more uniform circumferentially than either the total or static pressures individually.
6. For a constant value of fan rotational speed, increased cascade length (exit area) reduces all distortion parameters for the close-spacing configurations.
7. Changing the stator cascade spacing distance from 0.10 to 0.52 fan duct diameter essentially eliminates the fan inlet static pressure variation and the stator exit pressure variations.
8. To match the forward- and reverse-thrust operating points, an increase in the cascade length (exit area) is required for the close-spacing configurations compared to the extended-spacing configurations.



9. Use of the flight-type inlet alone reduces the overall performance compared to the bellmouth inlet plus recirculation shield configuration.

Lewis Research Center,  
National Aeronautics and Space Administration,  
Cleveland, Ohio, March 4, 1975,  
505-05.

#### REFERENCES

1. Dietrich, Donald A.; and Luidens, Roger W.: Experimental Performance of Cascade Thrust Reversers at Forward Velocity. NASA TM X-2665, 1973.
2. Gutierrez, O. A.; Stone, J. R.; and Friedman, R.: Results from Cascade Thrust Reverser Noise and Suppression Experiments. AIAA Paper 74-46, Jan-Feb. 1974.
3. Dietrich, D. A.; and Gutierrez, O. A.: Performance of a Model Cascade Thrust Reverser for Short-Haul Applications. AIAA Paper 74-1171, Oct. 1974.
4. Ammer, R. C.: Data Folder - STOL Reverser Scale Model Tests to Determine Effects of Reverser Axial Spacing and Extent of Circumferential Blockage on Performance and Fan Compatibility. TM-72-437, General Electric Co., 1972.
5. Ammer, R. C.: Data Folder - STOL Reverser Scale Model Tests to Determine Effects of Reverser Axial Spacing and Extent of Circumferential Blockage on Performance and Fan Compatibility - Addendum. TM-72-437-1, General Electric Co., 1972.
6. Performance of a 5.5-Inch Diameter Axial Fan with Various Inlets and Exits. Rep. 708-1, Tech Development, Inc., 1970.
7. Lopiccolo, Robert C.: Tests of Cascade Thrust Reversers on a 5.5-Inch Diameter Axial Fan. Rep. 789, Tech Development, Inc., 1971.
8. Lowe, W. H.; and Sanger, R. W.: Static Performance of a 13.97 cm (5.5 in.) Diameter Model VTOL Lift Fan. NASA CR-2051, 1972.
9. Dunavant, James C.; and Erwin, John R.: Investigation of a Related Series of Turbine-Blade Profiles in Cascade. NACA TN 3802, 1956.

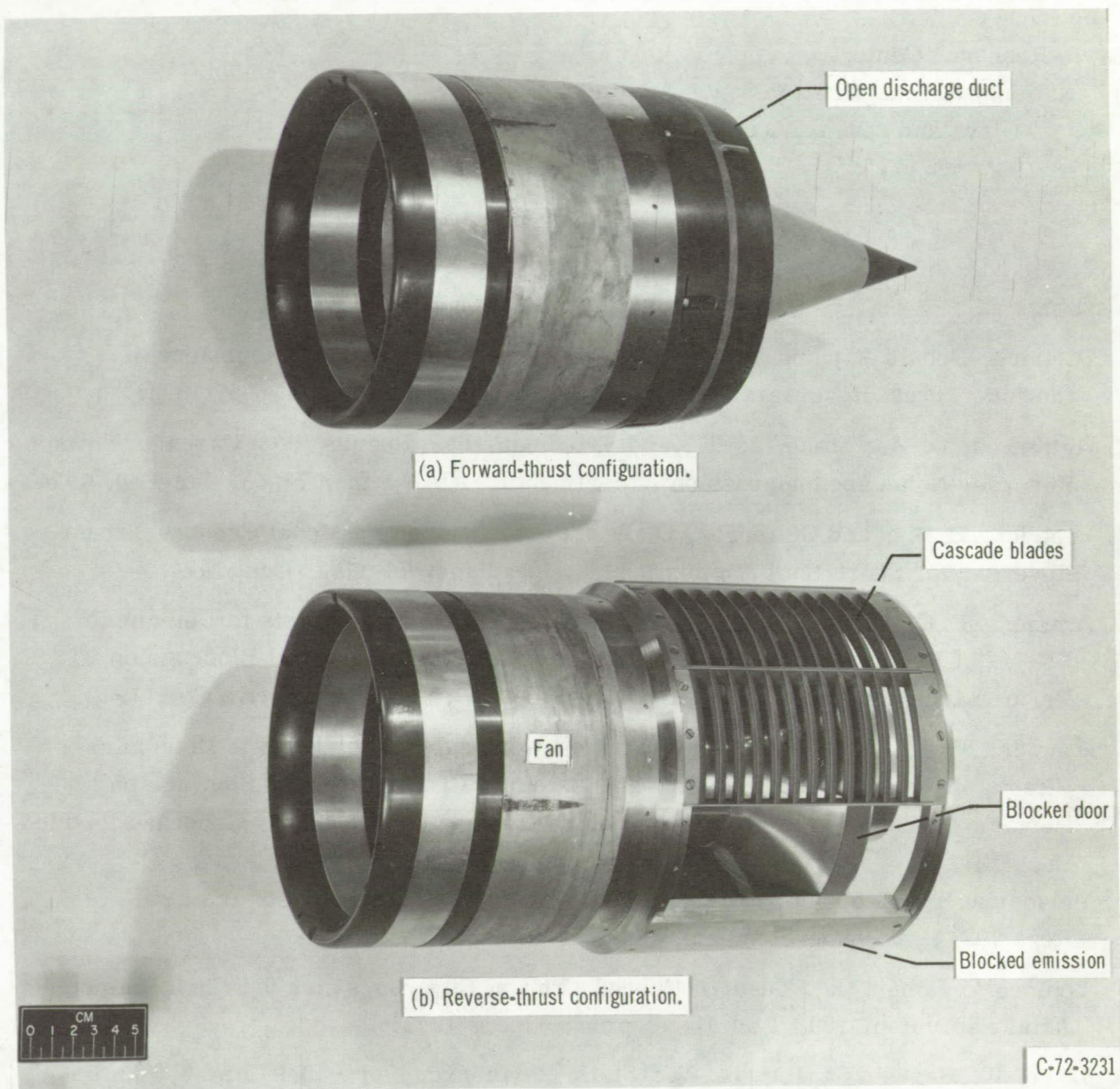
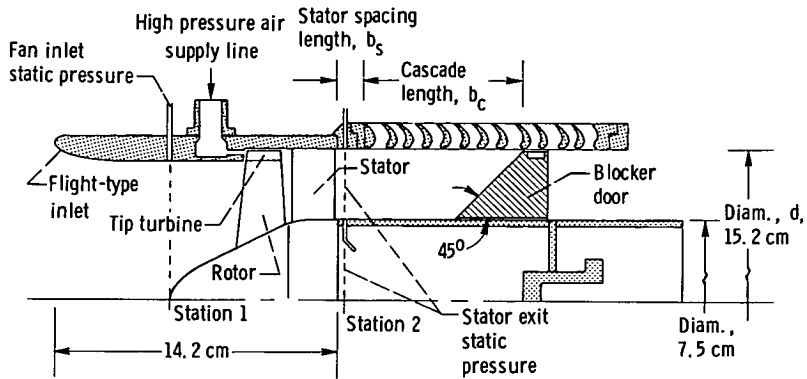
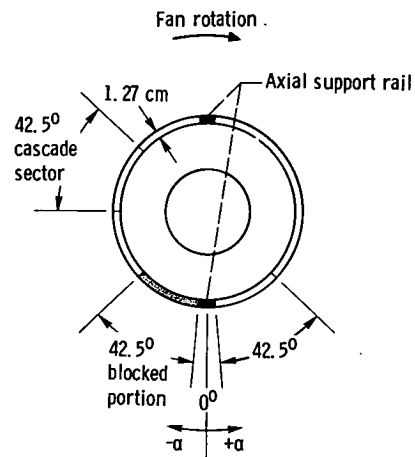


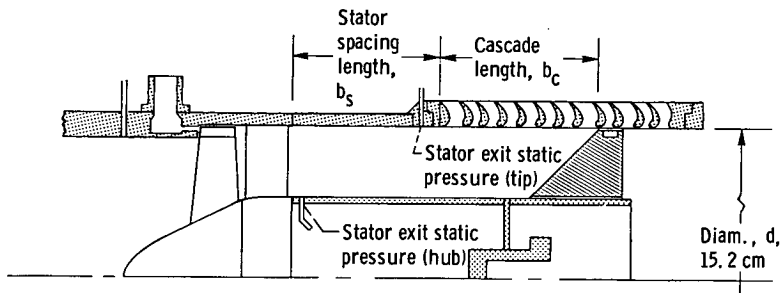
Figure 1. - Forward- and reverse-thrust models with flight-type inlet.



(a) Section of model with flight-type inlet and no stator-cascade spacer.



(b) Transverse section through reverser.



(c) Section of model with stator-cascade spacer.

Figure 2. - Fan reverser model.

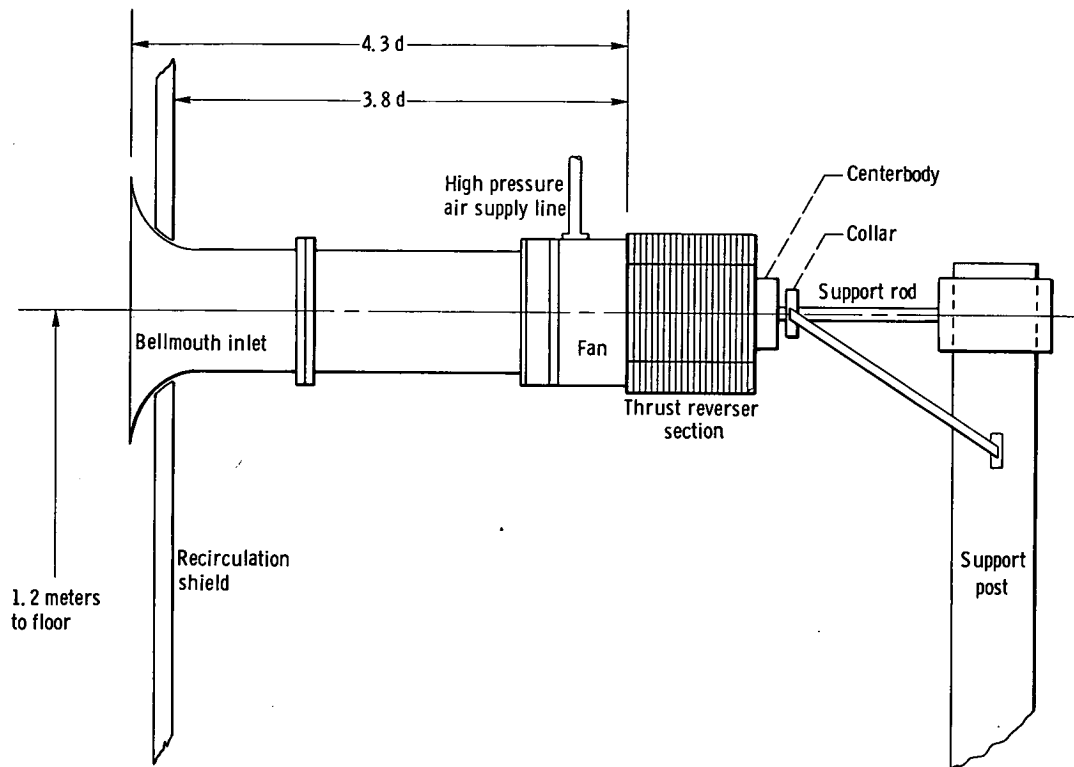


Figure 3. - Fan reverser model including bellmouth inlet and recirculation shield on static test stand.

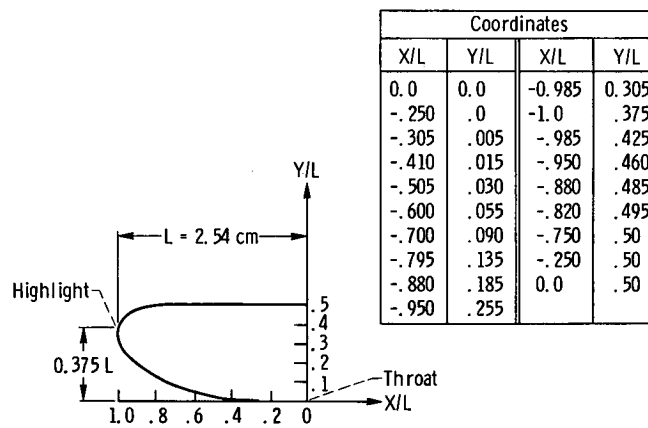


Figure 4. - Inlet lip design for flight-type inlet.

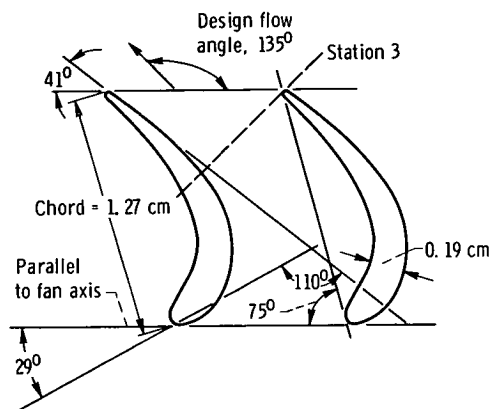


Figure 5. - Thrust-reverser blade section.

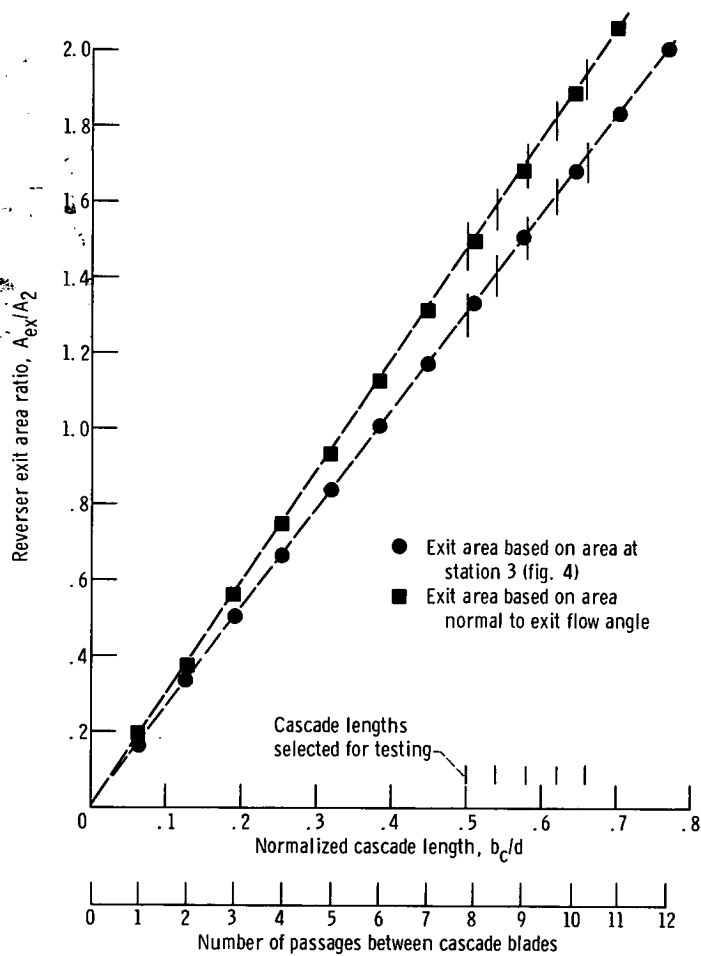


Figure 6. - Reverser exit area ratio variation as function of normalized cascade length.

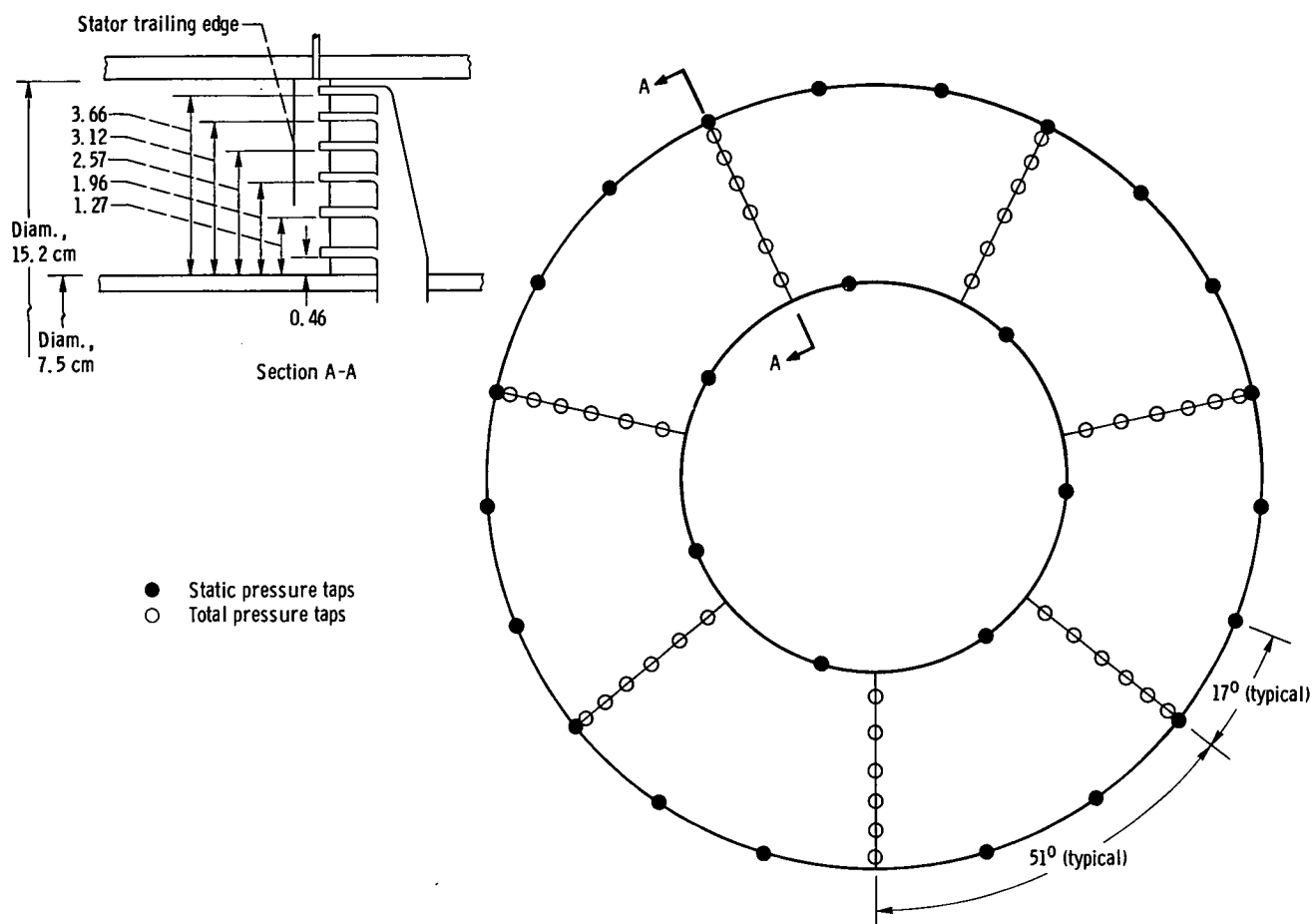


Figure 7. - Stator exit instrumentation schematic as viewed from downstream.

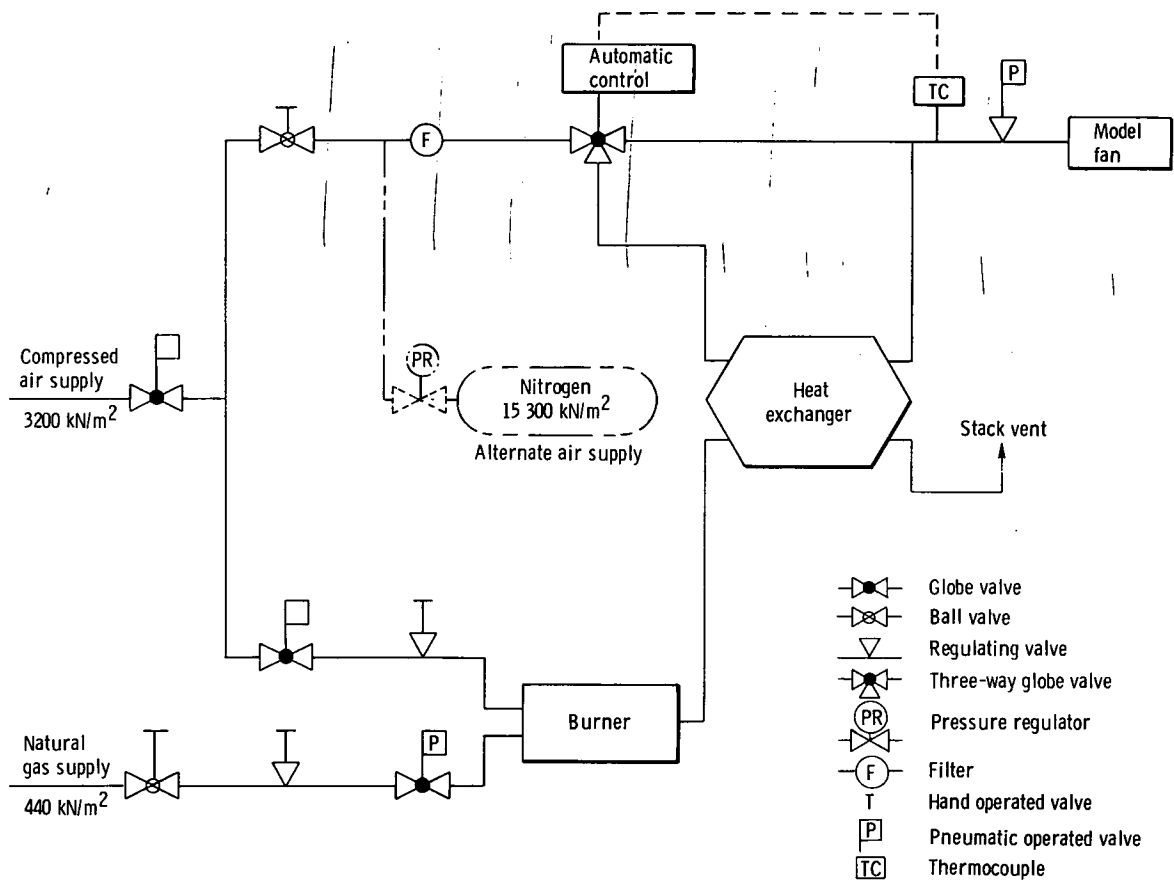
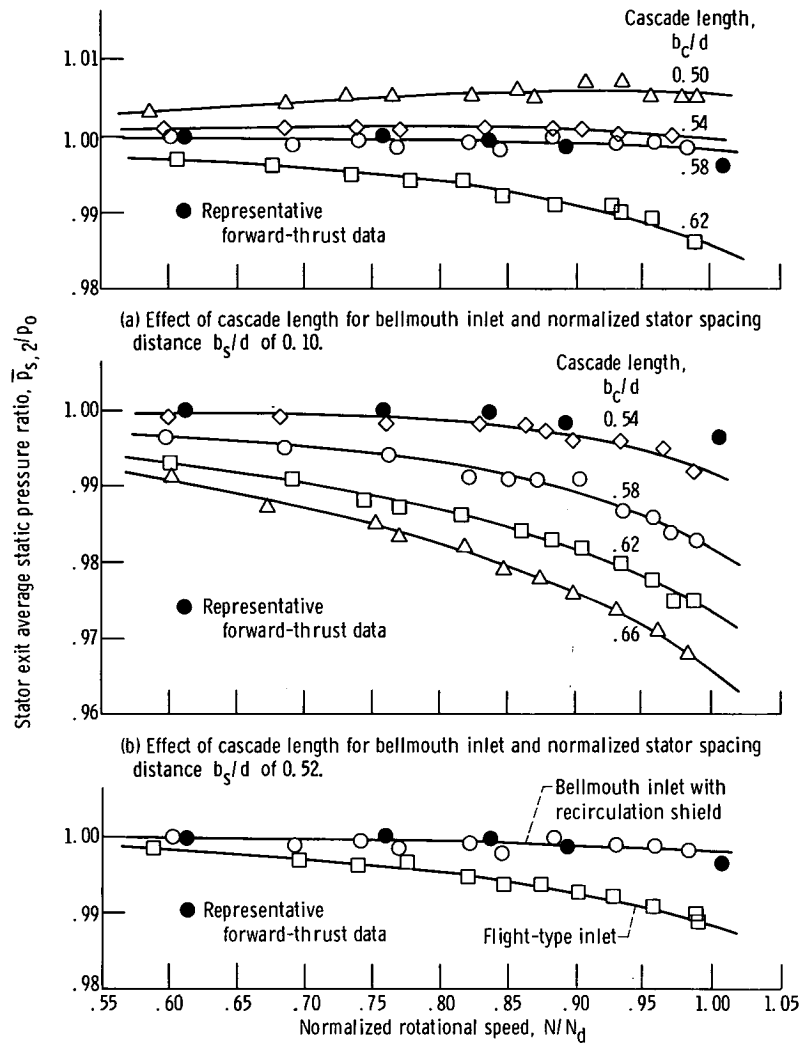


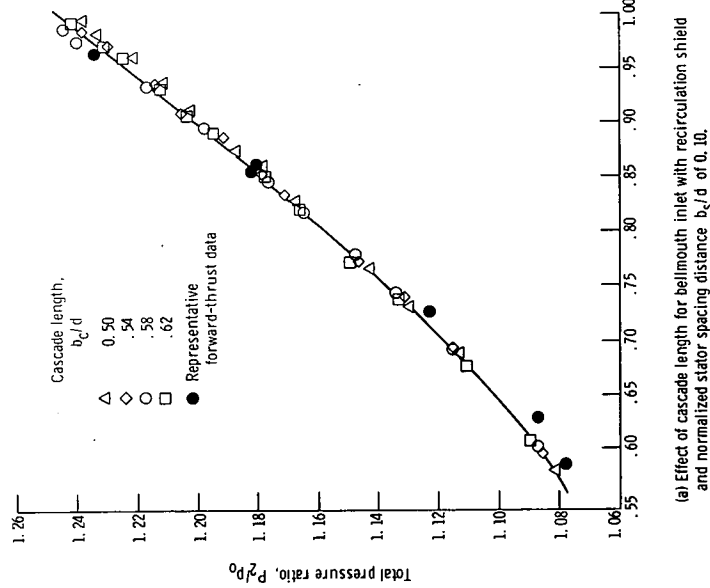
Figure 8. - Air supply system.



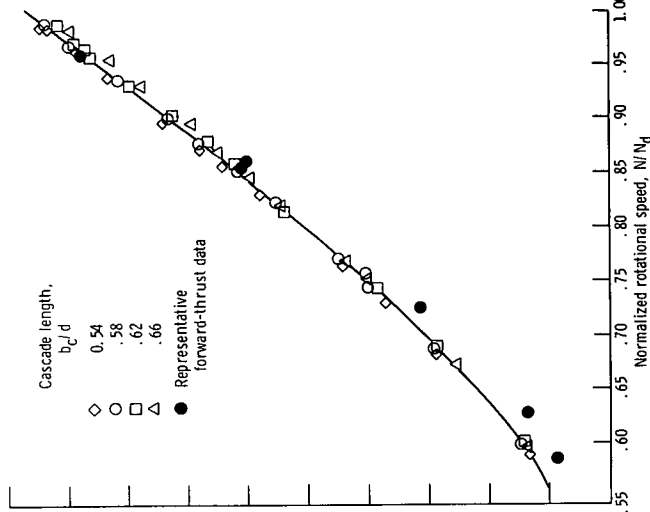
(c) Effect of cowl type for cascade length  $b_c/d$  of 0.58 and normalized stator spacing distance  $b_s/d$  of 0.10.

Figure 9. - Average stator exit static pressure ratio variation as function of normalized rotational speed.

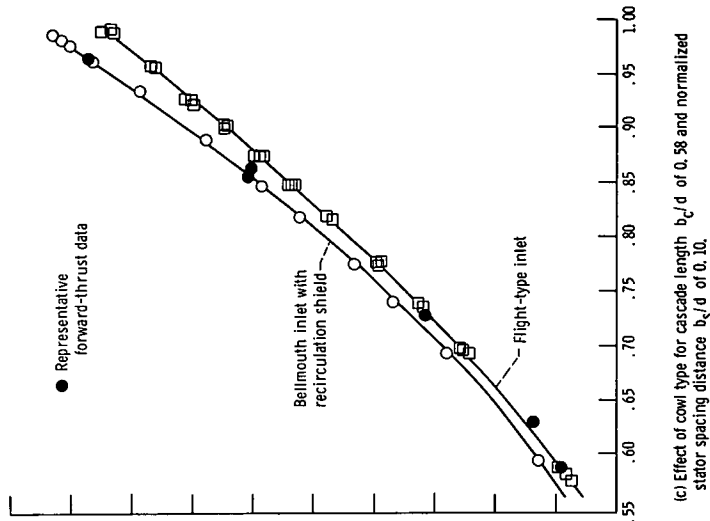




(a) Effect of cascade length for bellmouth inlet with recirculation shield and normalized stator spacing distance  $b_2/d$  of 0.10.

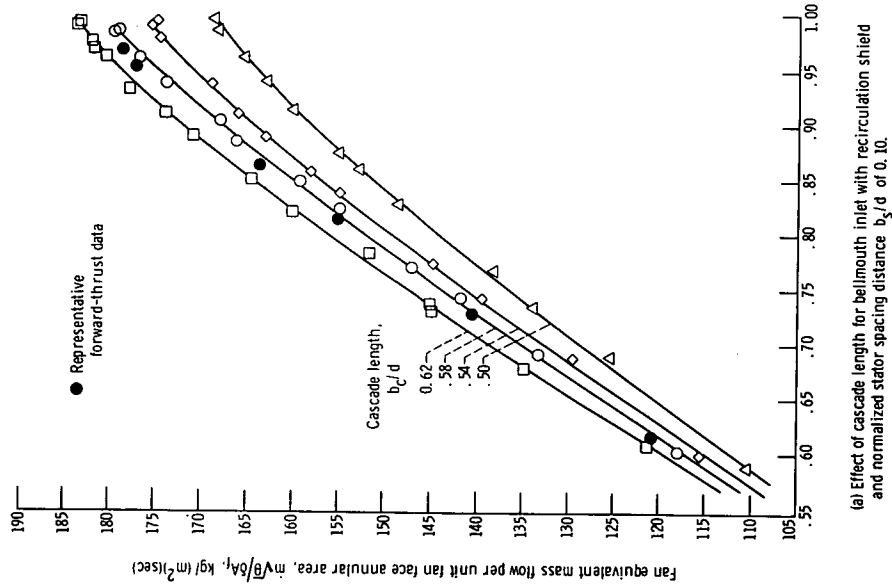


(b) Effect of cascade length for bellmouth inlet with recirculation shield and normalized stator spacing distance  $b_2/d$  of 0.52.

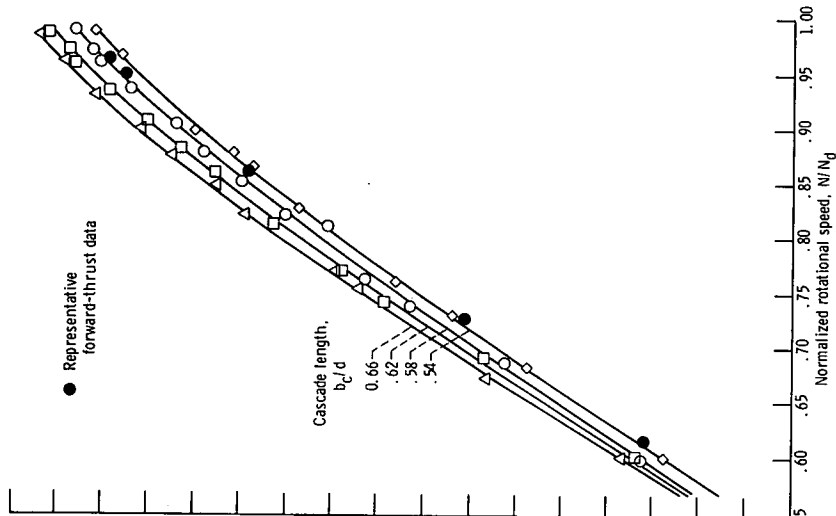


(c) Effect of cow type for cascade length  $b_c/d$  of 0.58 and normalized stator spacing distance  $b_2/d$  of 0.10.

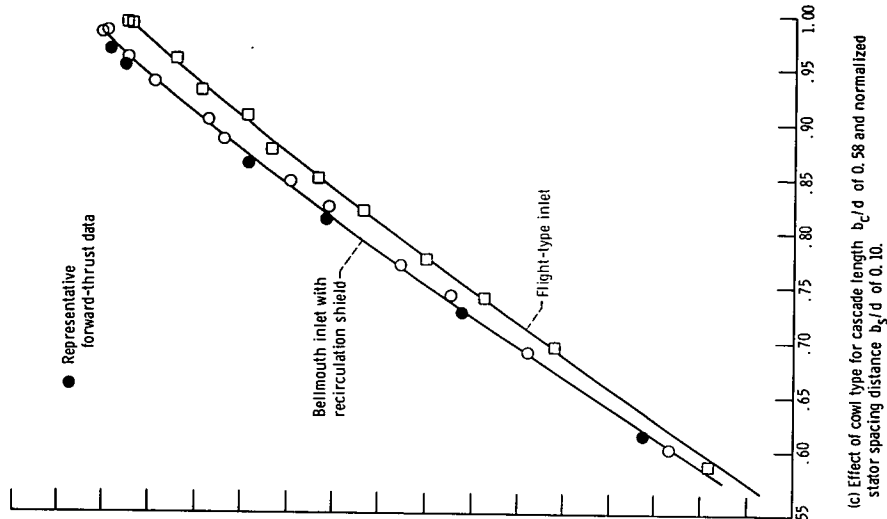
Figure 10. - Total pressure ratio variation as function of normalized rotational speed.



(a) Effect of cascade length for bellmouth inlet with recirculation shield and normalized stator spacing  $b_s/d$  of 0.10.

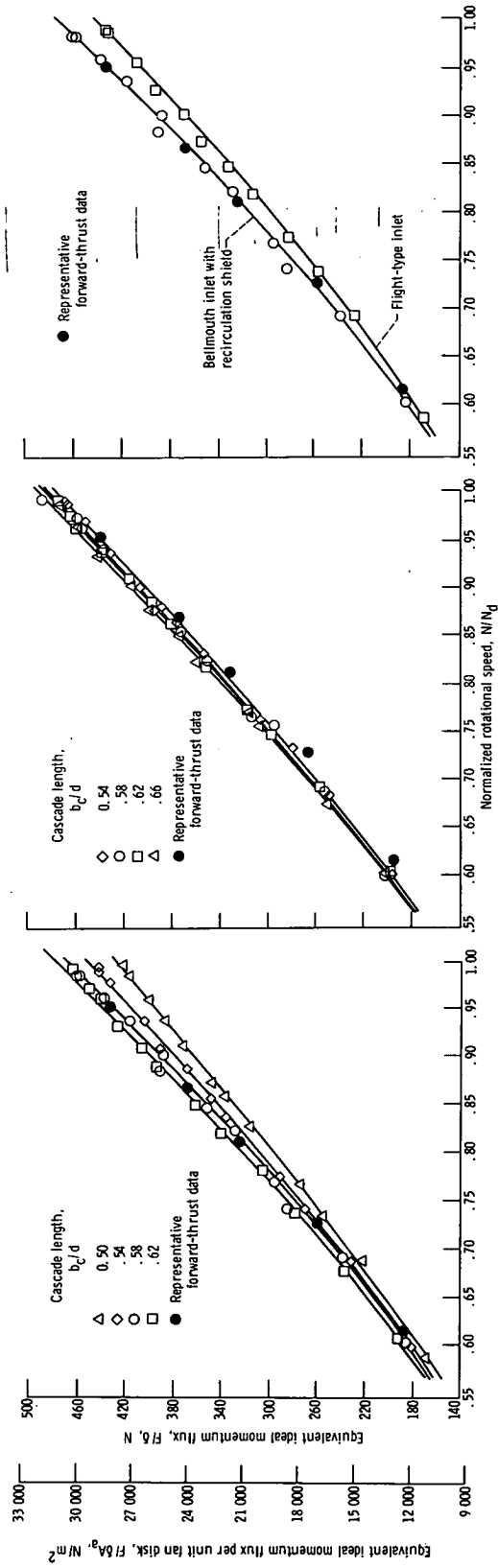


(b) Effect of cascade length for bellmouth inlet with recirculation shield and normalized stator spacing distance  $b_s/d$  of 0.52.



(c) Effect of cowl type for cascade length  $b_c/d$  of 0.58 and normalized stator spacing distance  $b_s/d$  of 0.10.

Figure 11. - Fan mass flow variation as function of normalized rotational speed.



(a) Effect of cascade length for bellmouth inlet with recirculation shield and normalized stator spacing distance  $b_2/d$  of 0.10.

(b) Effect of cascade length for bellmouth inlet with recirculation shield and normalized stator spacing distance  $b_2/d$  of 0.52.

(c) Effect of cowl type for cascade length  $b_2/d$  of 0.58 and normalized stator spacing distance  $b_2/d$  of 0.10.

Figure 12 - Corrected ideal thrust as function of normalized rotational speed.

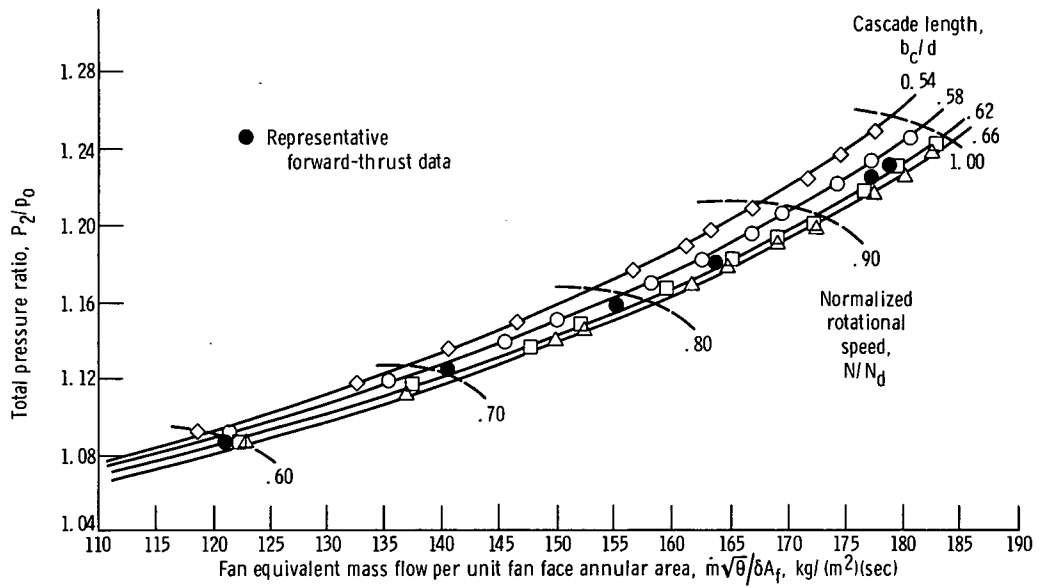
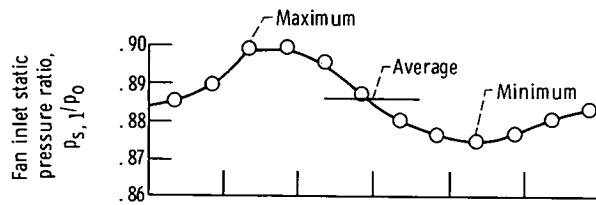
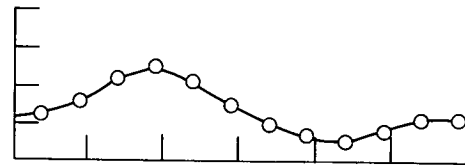


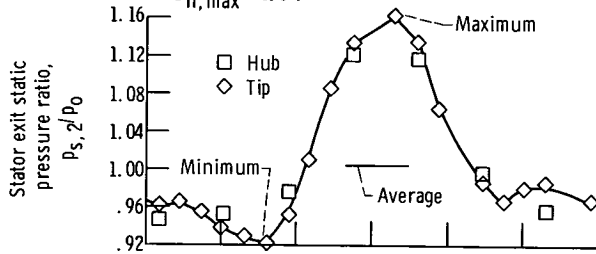
Figure 13. - Fan performance map for bellmouth inlet with recirculation shield and normalized stator spacing distance  $b_s/d$  of 0.52.



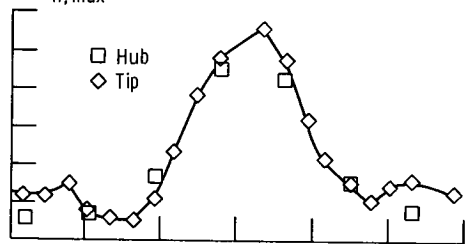
(a-1) Fan inlet static pressure distortion parameter  $D_{ff, \max} = 0.03$ .



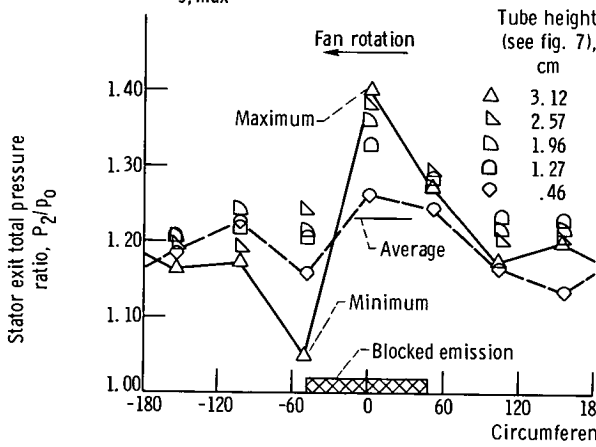
(b-1) Fan inlet static pressure distortion parameter  $D_{ff, \max} = 0.02$ .



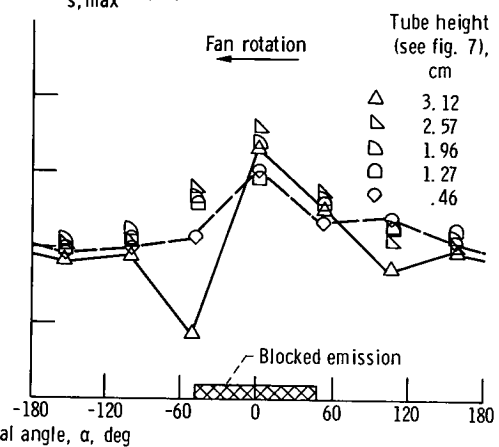
(a-2) Stator exit static pressure distortion parameter  $D_{s, \max} = 0.24$ .



(b-2) Stator exit static pressure distortion parameter  $D_{s, \max} = 0.21$ .



(a-3) Stator exit total pressure distortion parameter  $D_{t, \max} = 0.28$ .



(b-3) Stator exit total pressure distortion parameter  $D_{t, \max} = 0.22$ .

(a) Cascade length  $b_c/d = 0.50$ ; normalized rotational speed  $N/N_d = 0.98$ .

(b) Cascade length  $b_c/d = 0.54$ ; normalized rotational speed  $N/N_d = 0.98$ .

Figure 14. - Internal pressure profiles for bellmouth inlet with recirculation shield and normalized stator spacing distance  $b_s/d$  of 0.10.

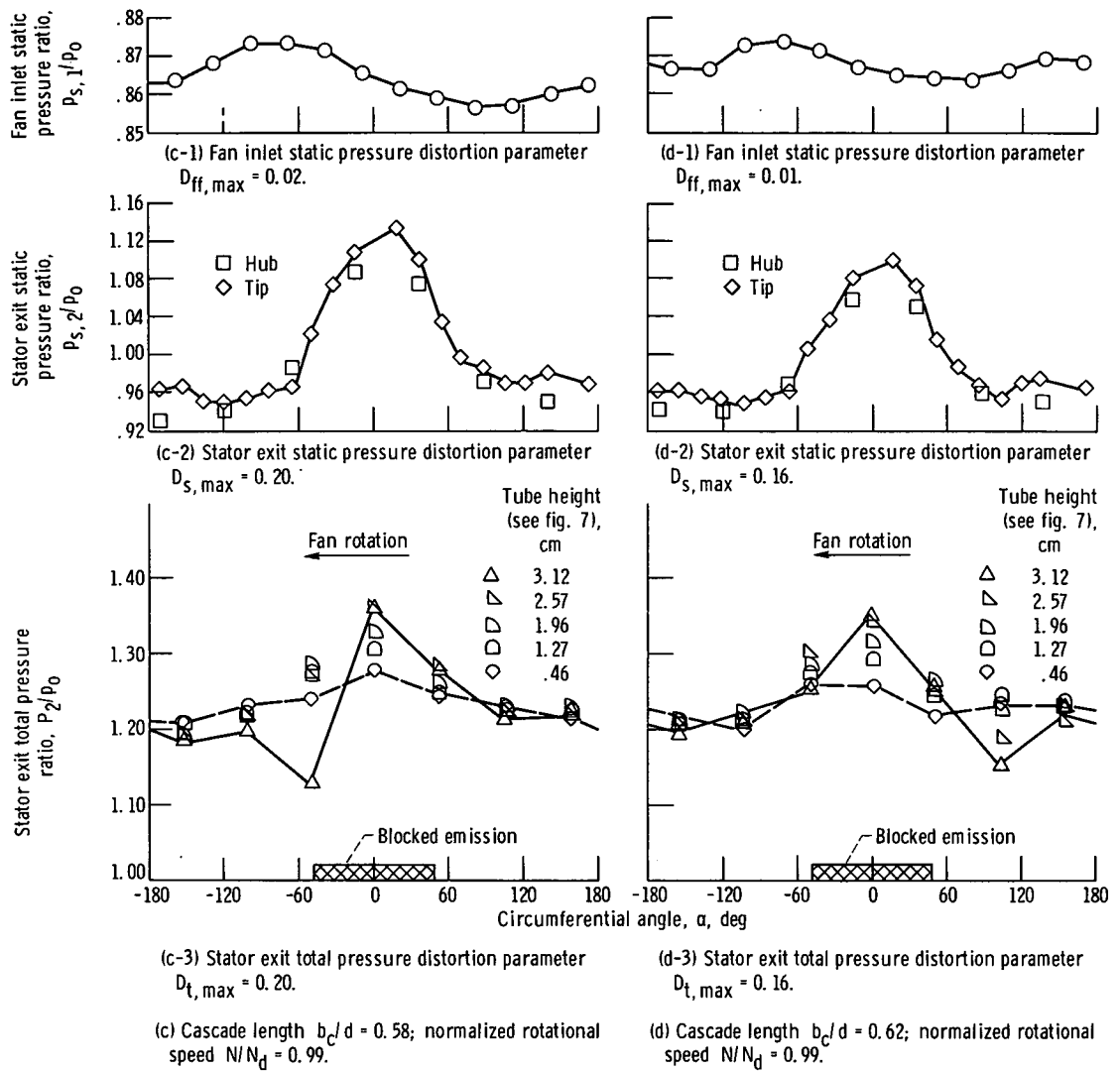


Figure 14. - Concluded.

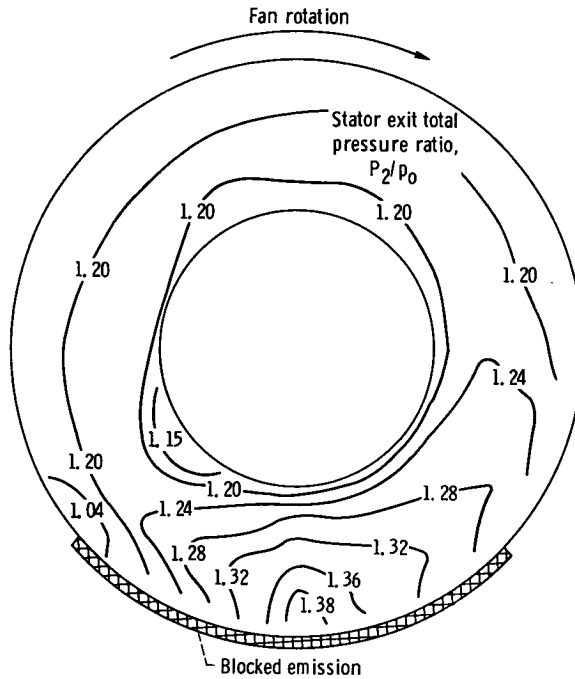


Figure 15. - Stator exit total pressure contours for bellmouth inlet with recirculation shield. Cascade length  $b_c/d = 0.50$ ; normalized stator spacing distance  $b_s/d = 0.10$ ; normalized rotational speed  $N/N_d = 0.98$ ; stator exit total pressure distortion parameter  $D_{t,max} = 0.28$ ; stator exit static pressure distortion parameter  $D_{s,max} = 0.24$ ; fan inlet static pressure distortion parameter  $D_{ff,max} = 0.03$ .

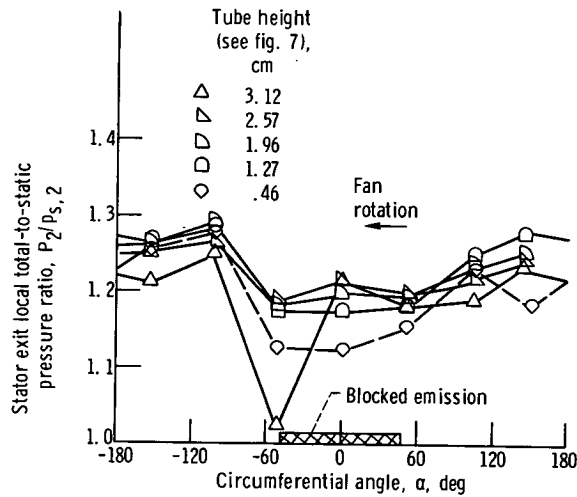
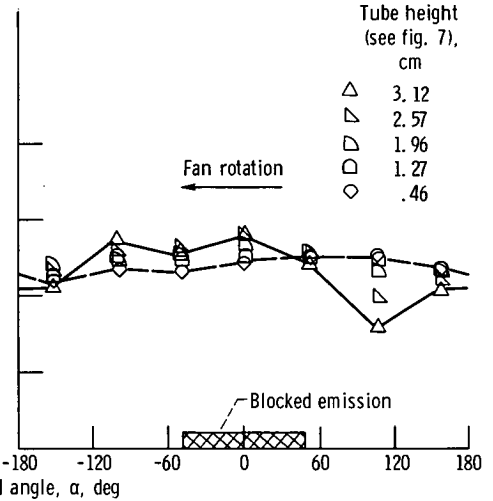
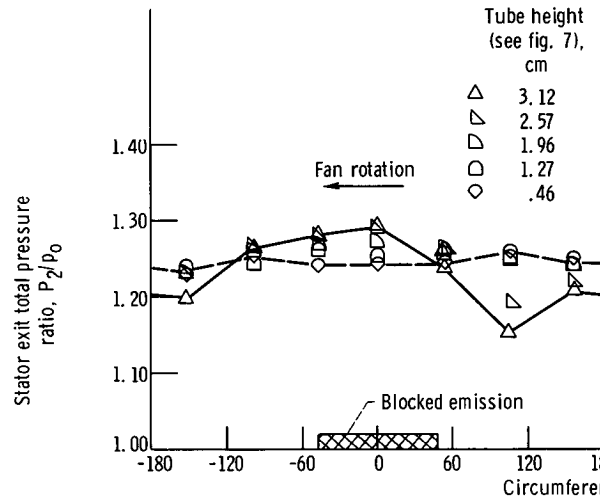
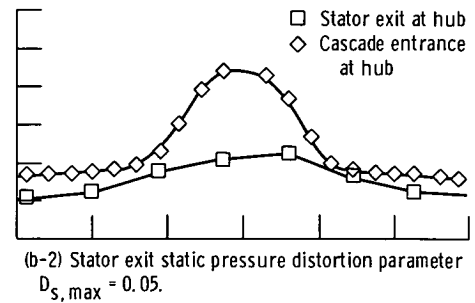
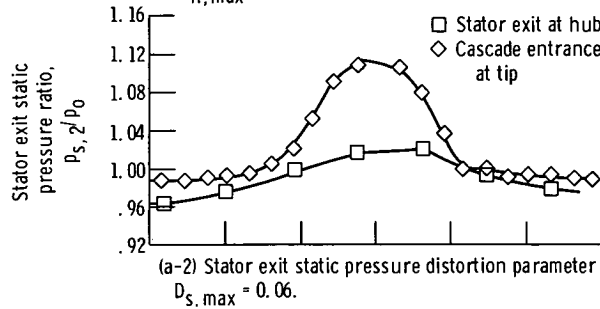
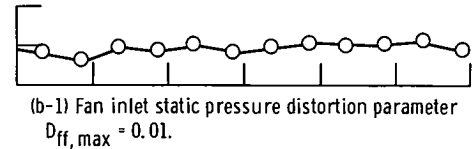
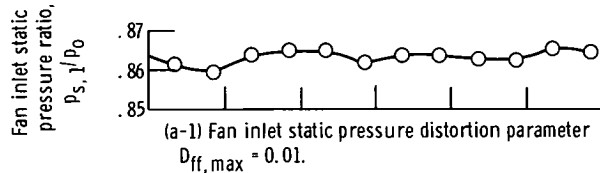


Figure 16. - Variation of local total-to-static pressure ratio at stator exit as function of circumferential angle for bellmouth inlet with recirculation shield. Cascade length  $b_c/d = 0.50$ ; normalized stator spacing distance  $b_s/d = 0.10$ ; normalized rotational speed  $N/N_d = 0.98$ .



(a) Cascade length  $b_c/d = 0.54$ ; normalized rotational speed  $N/N_d = 0.98$ .

(b) Cascade length  $b_c/d = 0.58$ ; normalized rotational speed  $N/N_d = 0.98$ .

Figure 17. - Internal pressure profiles for bellmouth inlet with recirculation shield and normalized stator spacing distance  $b_s/d$  of 0.52.



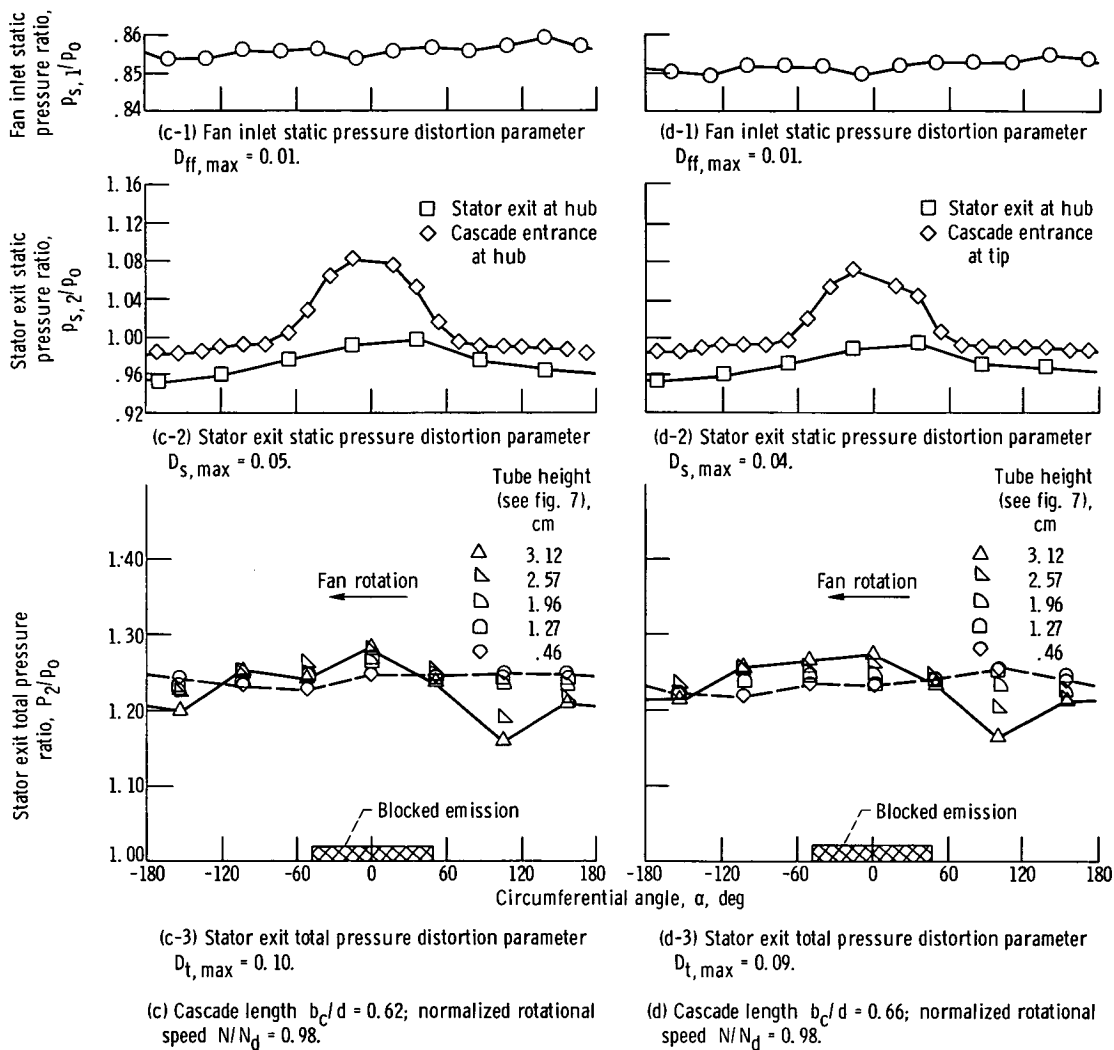


Figure 17. - Concluded.

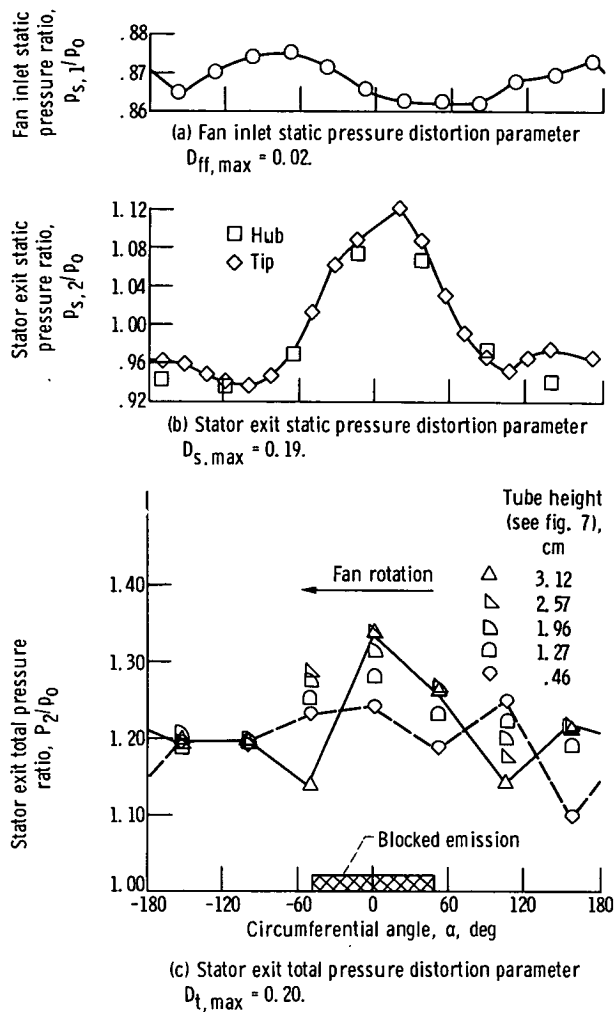
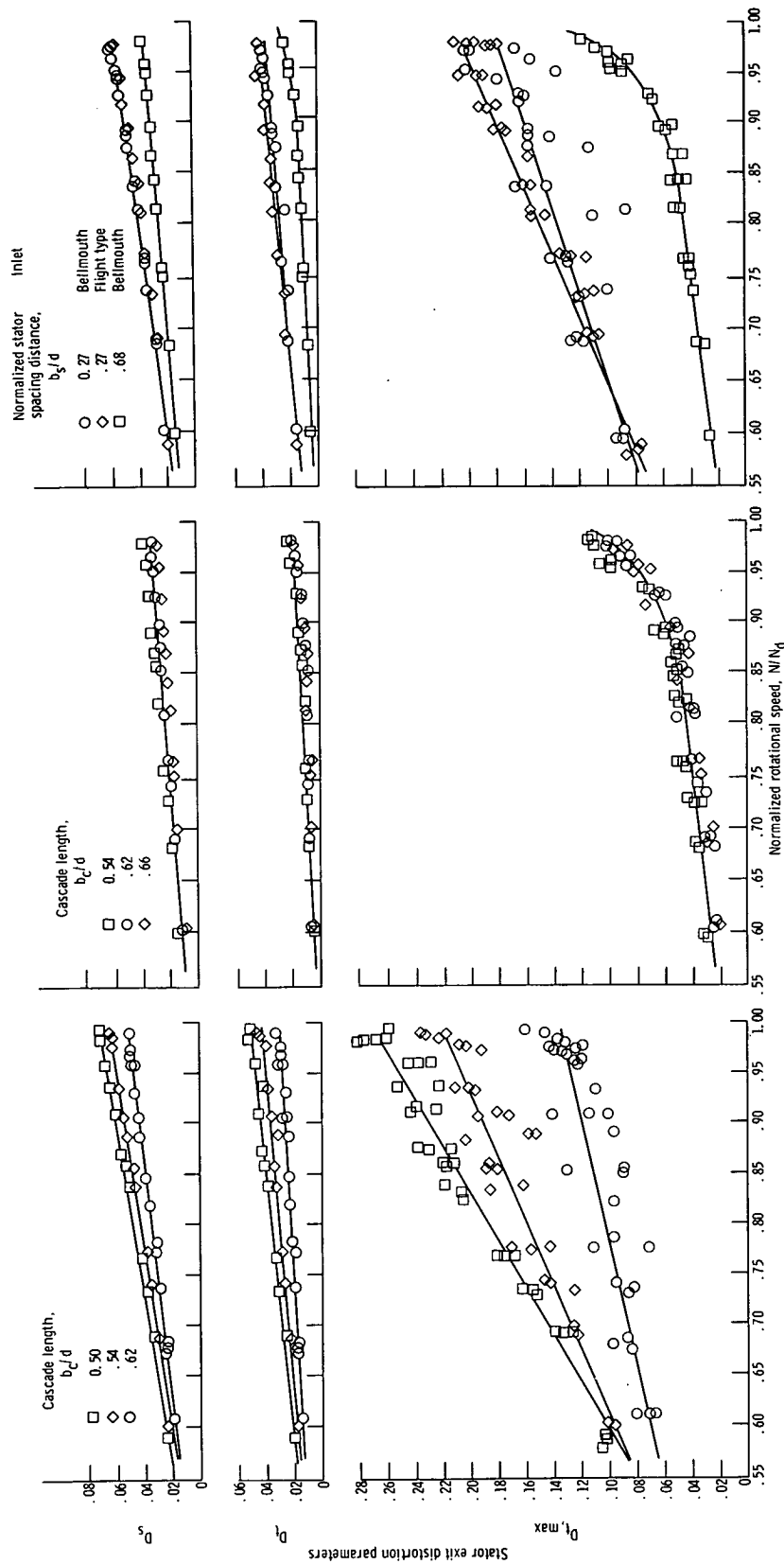


Figure 18. - Internal pressure profiles for flight-type inlet. Cascade length  $b_c/d = 0.58$ ; normalized stator spacing distance  $b_s/d = 0.10$ ; normalized rotational speed  $N/N_d = 0.99$ .



(a) Effect of cascade length for bellmouth inlet with recirculation shield and normalized stator spacing distance  $b_s/d$  of 0.10.  
 (b) Effect of cascade length for bellmouth inlet with recirculation shield and normalized stator spacing distance  $b_s/d$  of 0.52.  
 (c) Effect of inlet type and stator-to-cascade-inlet spacing for normalized cascade length  $b_c/d$  of 0.58.

Figure 19. - Variation of stator exit distortion parameters as function of normalized rotational speed for various tests.

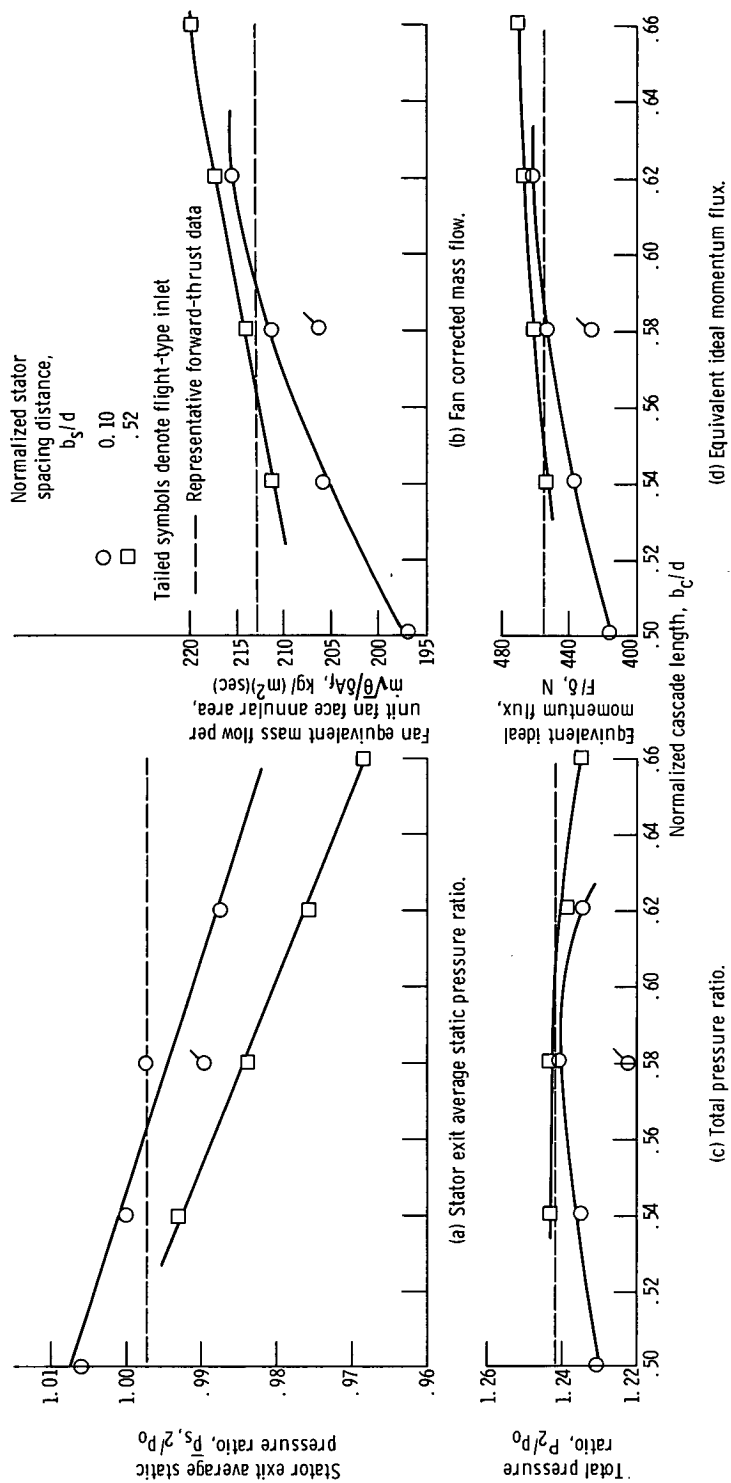


Figure 20. - Variation of fan characteristics as function of normalized cascade length for normalized rotational speed  $N/N_d = 0.98$ .

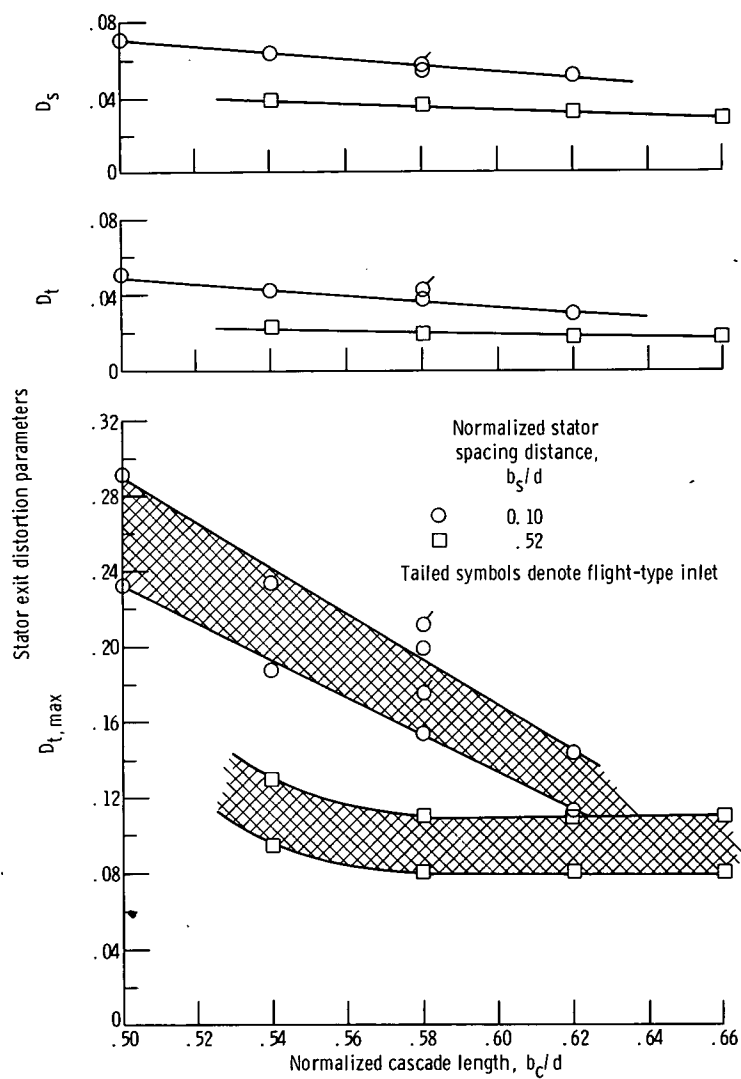


Figure 21. - Variation of stator exit distortion parameters as function of normalized cascade length for normalized rotational speed  $N/N_0$  of 0.98.



POSTMASTER: If Undeliverable (Section 158  
Postal Manual) Do Not Return

*"The aeronautical and space activities of the United States shall be conducted so as to contribute . . . to the expansion of human knowledge of phenomena in the atmosphere and space. The Administration shall provide for the widest practicable and appropriate dissemination of information concerning its activities and the results thereof."*

—NATIONAL AERONAUTICS AND SPACE ACT OF 1958

## NASA SCIENTIFIC AND TECHNICAL PUBLICATIONS

**TECHNICAL REPORTS:** Scientific and technical information considered important, complete, and a lasting contribution to existing knowledge.

**TECHNICAL NOTES:** Information less broad in scope but nevertheless of importance as a contribution to existing knowledge.

**TECHNICAL MEMORANDUMS:** Information receiving limited distribution because of preliminary data, security classification, or other reasons. Also includes conference proceedings with either limited or unlimited distribution.

**CONTRACTOR REPORTS:** Scientific and technical information generated under a NASA contract or grant and considered an important contribution to existing knowledge.

**TECHNICAL TRANSLATIONS:** Information published in a foreign language considered to merit NASA distribution in English.

**SPECIAL PUBLICATIONS:** Information derived from or of value to NASA activities. Publications include final reports of major projects, monographs, data compilations, handbooks, sourcebooks, and special bibliographies.

**TECHNOLOGY UTILIZATION PUBLICATIONS:** Information on technology used by NASA that may be of particular interest in commercial and other non-aerospace applications. Publications include Tech Briefs, Technology Utilization Reports and Technology Surveys.

*Details on the availability of these publications may be obtained from:*

**SCIENTIFIC AND TECHNICAL INFORMATION OFFICE  
NATIONAL AERONAUTICS AND SPACE ADMINISTRATION  
Washington, D.C. 20546**